et al., 2004,2006). Our simulation revealed a clear dependence of cardiac dysfunction on the area of the detubulated region. When the gap (detubulated region) was small, force generation was not appreciably affected due to the rapid propagation of the Ca^{2+} transient by diffusion and the slow time course of force development. By contrast, a large gap introduced a significant delay in the Ca^{2+} transient and in contraction in the detubulated region. Such dyssynchrony in contraction impairs the force generation and reduces the efficiency of contraction as the early contracting segment elongates the resting segment (internal shortening), thus wasting mechanical energy. These two factors may synergistically deteriorate cardiac function. In addition, our results suggest that the size of the detubulated region, together with t-tubule density, are the important factors for cardiomyocyte function, since the size of detubulation determines the delay of Ca^{2+} transient and the degree of inhomogeneity. In human heart failure there are

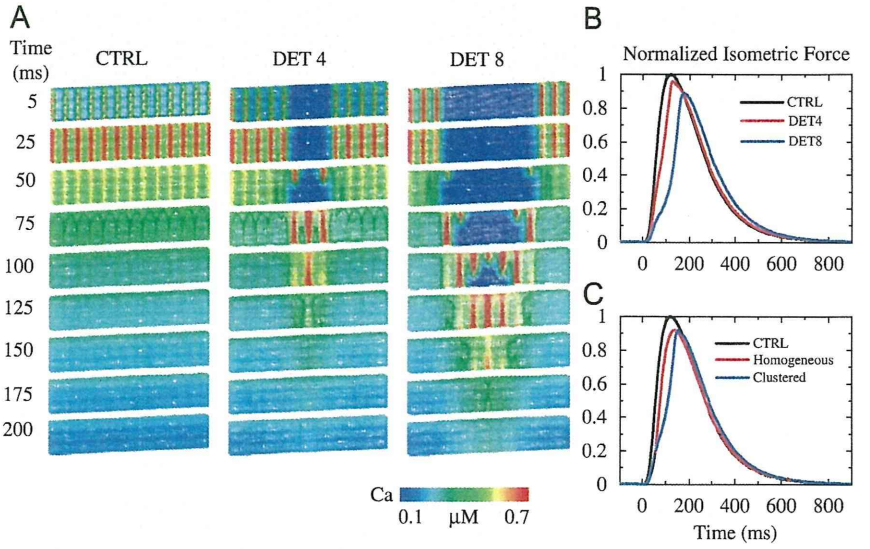

Fig. 7. Effect of regional detubulation on the Ca^{2+} transient and contraction. (A) Time-lapse images of $[Ca^{2+}]$ in color-coding during isometric contraction are shown for CTRL (left), DET4 (middle), and DET8 (right) myocytes. (B) Isometric forces are compared among the CTRL (black), DET4 (red), and DET8 (blue) myocytes. (C) Isometric forces are compared among the CTRL (black), homogeneous detubulation (red), and clustered detubulation (red). Forces are normalized for peak isometric value of CTRL in B and C.

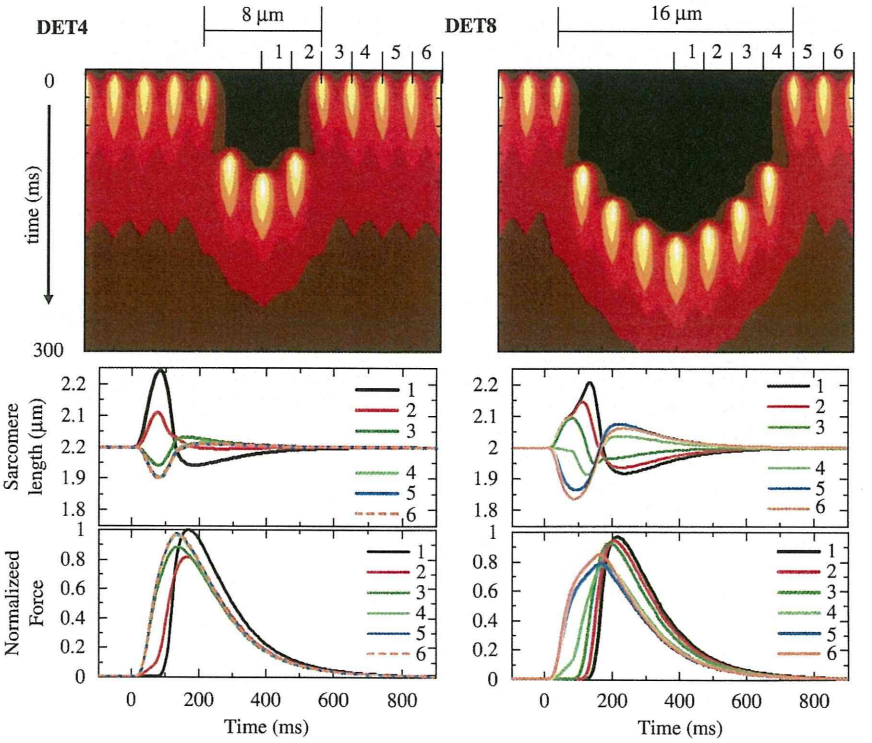

Fig. 8. Local Ca^{2+} transient and developed force of DET4 (left column) and DET8 (right column) models. Top rows: Longitudinal line-scan showing the local $[Ca^{2+}]$ with longitudinal position in horizontal axis and time after stimulus in vertical axis. Length change (middle rows) and developed force (bottom rows) of each sarcomere located in the position numbered in the longitudinal scan are shown.

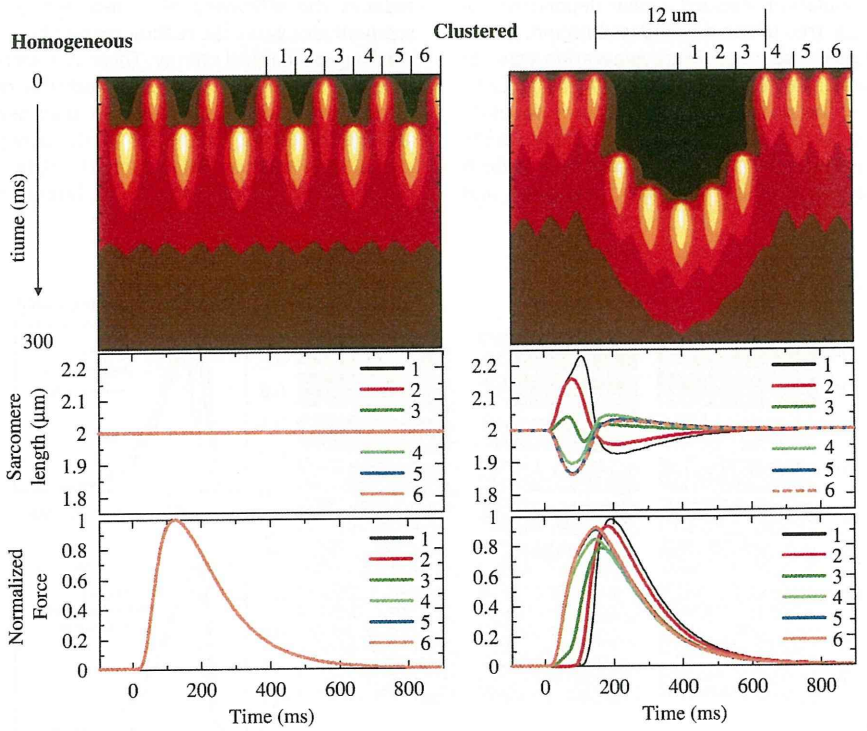

Fig. 9. Local Ca^{2+} transient and developed force of homogeneous (left column) and aggregated (right column) models. Top rows: Longitudinal line-scan showing the local $[Ca^{2+}]$ with longitudinal position in the horizontal axis and time after stimulus in the vertical axis. Length change (middle rows) and developed force (bottom rows) of each sarcomere located in the position numbered in the longitudinal scan are shown. In the homogeneous model, force and local $[Ca^{2+}]$ traces of each sarcomeres are superimposed.

large areas of t-tubule disorganization comparable to our large gap model (Fig. 5 of (Cannell et al., 2006)). However, in the murine model of heart failure the majority of the delayed Ca^{2+} release region had a width of less than 4 μm (Louch et al., 2006). Nevertheless, even with such small gaps in the t-tubule system, concomitant alterations in Ca^{2+} handling proteins can induce cardiac dysfunction. In this study, however, we only evaluated the effect of t-tubule disorganization.

4.3. Limitations of the model

For our model, we used both detailed single-sarcomere models and 12-sarcomere models with coarse mesh. However, even with the coarse mesh model, the analysis volume was insufficient to impose a three-dimensionally inhomogeneous deformation. A whole cell model with a more realistic sub-cellular structure is required for further analysis, although compromising the computational cost would be a prerequisite for such modeling. On the other hand, uncertainty in the subcellular distributions of functional components including ion channels also limits the analysis (Pasek et al., 2008). The modeling study can be used to estimate these unknown parameters, although further experimental clarification and verification are required. Finally, we assumed that the $[Ca^{2+}]$ of the t-tubular space was equal to that of bulk extracellular space. However, the $[Ca^{2+}]$ of t-tubular space was estimated to decrease by 13.8% at onset of Ca^{2+} release under pacing at 1 Hz (Pasek et al., 2008). The diffusion process in the extracellular space needs to be implemented in future model development.

Conflict of interest statement

None.

Acknowledgments

This research was supported by the Japan Society for the Promotion of Science (JSPS) through its Research Fellowships for Young Scientists (A.H.) and through its Funding Program for World-Leading Innovative R&D on Science and Technology FIRST Program (A.H., J.O., T.W., S.S., and T.H.), and JSPS KAKENHI (B) (20300152) (S.S.). This research was also supported by the Japan Science and Technology Agency (JST) through its University-Industry Collaborative Grants Fostering Innovation in Technology-Seeds.

Appendix A. Supplementary Information

Supplementary data associated with this article can be found in the online version at doi:10.1016/j.jbiomech.2011.11.022.

References

Aliev, M.K., Dos Santos, P., Hoerter, J.A., Soboll, S., Tikhonov, A.N., Saks, V.A., 2002. Water content and its intracellular distribution in intact and saline perfused rat hearts revisited. Cardiovascular Research 53, 48–58.

Bers, D.M., 2001. Ca source and Sinks. Excitation–Contraction Coupling and Cardiac Contractile Force, 2nd ed. Kluwer Academic Publishers, Dordrecht, The Netherlands.

Bers, D.M., 2006. Altered cardiac cyocyte Ca regulation in heart failure. Physiology 21, 380–387.

Brette, F., Despa, S., Bers, D.M., Orchard, C.H., 2005. Spatiotemporal characteristics of SR Ca^{2+} uptake and release in detubulated rat ventricular myocytes. Journal of Molecular and Cellular Cardiology 39, 804–812.

Brette, F., Komukai, K., Orchard, C.H., 2002. Validation of formamide as a detubulation agent in isolated rat cardiac cells. American Journal of Physiology 283, H1720–H1728.

Brette, F., Orchard, C., 2003. T-tubule function in mammalian cardiac myocytes. Cardiovascular Research 92, 1182–1192.
Brette, F., Rodriguez, P., Komukai, K., Colyer, J., Orchard, C.H., 2004. β-adrenergic stimulation restores the Ca transient of ventricular myocytes lacking t-tubule. Journal of Molecular and Cellular Cardiology 36, 265–275.
Cannell, M.B., Crossman, D.J., Soeller, C., 2006. Effects of changes in action potential spike configuration, junctional sarcoplasmic reticulum micro-architecture and altered t-tubule structure in human heart failure. Journal of Muscle Research and Cell Motility 27, 297–306.
Chen-Izu, Y., McCulle, S.L., Ward, C.W., Soeller, C., Allen, B.M., Rabang, C., Cannell, M.B., Balke, C.W., Izu, L.T., 2006. Three-dimensional distribution of ryanodine receptor clusters in cardiac myocytes. Biophysical Journal 91, 1–13.
Cheng, Y., Yu, Z., Hoshijima, M., Holst, M.J., McCulloch, A.D., McCammon, J.A., Michailova, A.P., 2010. Numerical analysis of Ca^{2+} signaling in rat ventricular myocytes with realistic transverse-axial tubular geometry and inhibited sarcoplasmic reticulum. PLoS Computational Biology 6, e1000972.
Cortassa, S., Aon, M.A., O'Rourke, B., Jacques, R., Tseng, H.-J., Marban, E., Winslow, R.L., 2006. A computational model integrating electrophysiology, contraction, and mitochondrial bioenergetics in the ventricular myocyte. Biophys J 91, 1564–1589.
de Graaf, R.A., van Kranenburg, A., Nicolay, K., 2000. In Vivo ^{31}P-NMR diffusion spectroscopy of ATP and phosphocreatine in rat skeletal muscle. Biophysical Journal 78, 1657–1664.
Dibb, K.M., Clarke, J.D., Horn, M.A., Richards, M.A., Graham, H.K., Eisner, D.A., Trafford, A.W., 2009. Characterization of an extensive transverse tubular network in sheep atrial myocytes and its depletion in heart failure. Circulation: Heart Failure, 482–489.
Greenstein, J.L., Hinch, R., Winslow, R.L., 2006. Mechanisms of excitation–contraction coupling in an integrative model of the cardiac ventricular myocyte. Biophysical Journal 90, 77–91.
Harris, D.M., Mills, G.D., Chen, X., Kubo, H., Berretta, R.M., Votaw, V.S., Santana, L.F., Houser, S.R., 2005. Alterations in early action potential repolarization causes localized failure of sarcoplasmic reticulum Ca^{2+} release. Circulation Research 96, 543–550.
Heinzel, F.R., Bito, V., Biesmans, L., Wu, M., Detre, E., von Wegner, F., Claus, P., Dymarkowski, S., Maes, F., Bogaert, J., Rademakers, F., D'hooge, J., Sipido, K., 2008. Remodeling of T-tubules and reduced synchrony of Ca^{2+} release in myocytes from chronically ischemic myocardium. Circulation Research 102, 338–346.
Ibrahim, M., Al Masri, A., Navaratnarajab, M., Siedlecka, U., Scopa, G.K., Moshkov, A., Al-Saud, S.A., Gorelik, J., Yacoub, M.H., Terraciano, C.M.N., 2010. Prolonged mechanical unloading affects cardiomyocyte excitation–contraction coupling, transverse-tubule structure, and the cell surface. FASEB Journal 24, 321–3329.
Kawai, M., Hussain, M., Orchard, C.H., 1999. Excitation–contraction coupling in rat ventricular myocyte after formamide-induced detubulation. American Journal of Physiology 277, H603–H609.
Kirk, M.M., Izu, L.T., Chen-Izu, Y., McCulle, S.L., Wier, W.G., Balke, C.W., Shorofsky, S.R., 2003. Role of the transverse-axial tubule system in generating calcium sparks and calcium transients in rat atrial myocytes. Journal of Physiology 547, 441–451.
Livshitz, L.M., Rudy, Y., 2007. Regulation of Ca^{2+} and electrical alternans in cardiac myocytes: role of CAMKII and repolarizing currents. American Journal of Physiology – Heart and Circulatory Physiology 292, H2854–H2866.
Louch, W.E., Bito, V., Heinzel, F.R., Macianskiene, R., Vanhaecke, J., Flameng, W., Mubagwa, K., Sipido, K.R., 2004. Reduced synchrony of Ca^{2+} release with loss of T-tubules – a comparison to Ca^{2+} release in human failing cardiomyocyte. Cardiovascular Research 62, 63–73.
Louch, W.E., Mork, H.K., Sexton, J., Stromme, T.A., Laake, P., Sjaastad, I., Sejersted, O.M., 2006. T-tubule disorganization and reduced synchrony of Ca^{2+} release in murine cardiomyocytes following myocardial infarction. Journal of Physiology 574, 519–533.
Lukyanenko, V., Chikando, A., Lederer, W.J., 2009. Mitochondria in cardiomyocyte Ca^{2+} signaling. The International Journal of Biochemistry & Cell Biology 41, 1957–1971.
Negroni, J.A., Lascano, E.C., 1996. A cardiac muscle model relating Sarcomere dynamics to calcium kinetics. Journal of Molecular and Cellular Cardiology 28, 915–929.
Okada, J., Sugiura, S., Nishimura, S., Hisada, T., 2005. Three-dimensional simulation of calcium waves and contraction in cardiomyocytes using the finite element method. American Journal of Physiology 288, 510–522.
Orchard, C., Brette, F., 2008. t-tubules and sarcoplasmic reticulum function in cardiac ventricular myocytes. Cardiovascular Research 77, 237–244.
Pasek, M., Simurda, J., Orchard, C.H., Christe, G., 2008. A model of the guinea-pig ventricular cardiac myocyte incorporating a transverse-axial tubular system. Progress in Biophysics and Molecular Biology 96, 258–280.
Smyrnias, I., Mair, W., Harzheim, D., Walker, S.A., Roderick, H.L., Bootman, M.D., 2010. Comparison of the T-tubule system in adult rat ventricular and atrial myocytes, and its role in excitation–contraction coupling and inotropic stimulation. Cell Calcium 47, 210–223.
Song, L.-S., Sobie, E.A., McCulle, S., Lederer, W.J., Balke, C.W., Cheng, H., 2006. Orphaned ryanodine receptors in the failing heart. Proceedings of the National Academy of Sciences of the United States of America 103, 4305–4310.
Stern, M.D., 1992. Theory of excitation–contraction coupling in cardiac muscle. Biophysical journal 63, 497–517.
Vendelin, M., Birkedal, R., 2008. Anisotropic diffusion of fluorescently labeled ATP in rat cardiomyocytes determined by raster image correlation spectroscopy. American Journal of Physiology 295, C1302–C1315.
Watanabe, H., Sugiura, S., Kafuku, H., Hisada, T., 2004. Multiphysics simulation of left ventricular filling dynamics Using fluid–structure interaction. Finite Element Method 87, 2074–2085.
Wei, S., Guo, A., Chen, B., Kutschke, W., Xie, Y.-P., Zimmerman, K., Weiss, R.M., Anderson, M.E., Cheng, H., Song, L.-S., 2010. T-tubule remodeling during transition from hypertrophy to heart failure. Circulation Research 107, 520–531.
Yang, A., Pascarel, C., Steele, D.S., Komukai, K., Brette, F., Orchard, C.H., 2002. Na^{+}–Ca^{2+} exchanger activity is localized in the T-tubules of rat ventricular myocytes. Circulation Research 91, 315–322.
Yu, Z., Yao, G., Hoshijima, M., Michailova, A., Holst, M., 2011. Multi-scale modeling of calcium dynamics in ventricular myocytes with realistic transverse tubules. Biomedical Engineering, IEEE Transactions on PP. 1-1.

33rd Annual International Conference of the IEEE EMBS
Boston, Massachusetts USA, August 30 - September 3, 2011

Reduction of Myocardial Oxygen Demand by Controlling Heart Rate and Hemodynamics Simultaneously by Novel Circulatory Model

Masaru Sugimachi, *Member, IEEE*, Kazunori Uemura, Toru Kawada, Toshiaki Shishido, and Kenji Sunagawa, *Member, IEEE*

Abstract—**We were already capable of restoring automatically blood pressure, cardiac output, and left atrial pressure by an inotropic, a vasodilator, and volume infusion/a diuretic. Countermeasures for cardioprotection, however, should be integrated to improve the long-term outcomes. We established a full control of heart rate and examined if such a control was useful for decreasing cardiac oxygen consumption. Based on a simulation result, we conducted an animal experiment. In 7 dogs with acute heart failure, we treated hemodynamics, and then lowered heart rate. Compared to the treatment for hemodynamics alone, the addition of bradycardia decreased cardiac oxygen consumption. It was possible to maintain hemodynamics without sacrificing cardiac oxygen consumption.**

I. Introduction

THE ultimate goal of the treatment of acute failure is the restoration of failing hemodynamics. Although the native regulation for the cardiovascular system plays a role to sustain normal blood pressure when the severity of heart failure is mild (called compensated heart failure), the ability of native regulation is limited. To sustain life, not only blood pressure, but also peripheral perfusion (indexed by cardiac output) and the absence of pulmonary edema (indexed by low left atrial pressure) are necessary. The native regulation fails to restore cardiac output and left atrial pressure in advanced heart failure.

We have shown that with the use of an inotropic agent, a vasodilator, and volume infusion/a diuretic, we were able to restore automatically all of blood pressure, cardiac output, left atrial pressure [1]. In this study, the peripheral demand was fulfilled. The overload on the heart was, however, not ameliorated. Countermeasures for cardioprotection should probably also be a part of the treatment and should be integrated, so as to improve the long-term outcomes of the patient recovering from acute heart failure.

Manuscript received April 13, 2011. This work was supported in part by Grant-in-Aid for Scientific Research (B 20300164) from the Ministry of Education, Culture, Sports, Science and Technology, by Health and Labour Sciences Research Grants (H20-katsudo-shitei-007) from the Ministry of Health Labour and Welfare of Japan (corresponding author Masaru Sugimachi, MD, PhD to provide phone: +81-6-6833-5012; fax: +81-6-6835-5403; e-mail: su91mach@ri.ncvc.go.jp).

M. Sugimachi, K. Uemura, T. Kawada, and T. Shishido are with the National Cerebral and Cardiovascular Center Research Institute, Suita, Osaka 5658565, Japan.

K. Sunagawa is with Kyushu University, Fukuoka 8128582 Japan.

We have already used the control of left ventricular contractility, systemic vascular resistance and blood volume to automatically restore blood pressure, cardiac output, and left atrial pressure. For the cardioprotection, we have to use the control of another cardiovascular property. We focused on the control of heart rate and examined if this was useful for the cardioprotection. We assumed here that low minute left ventricular oxygen consumption can be used as an index for cardioprotection.

II. Theoretical Analysis

A. Definition of the Problem

To supply the peripheral demand and to prevent pulmonary congestion, the cardiovascular system needs to operate with sufficiently high mean blood pressure (P_m), large cardiac output (CO), and low left atrial pressure (P_{LA}). Considering the physiologically normal values, we fixed P_m to 100 mmHg, CO to 100 $ml \cdot min^{-1} \cdot kg^{-1}$, and P_{LA} to 10 mmHg.

Even with these multiple constraints, the cardiovascular system does not operate with a unique condition. It can operate with various sets of contractility and heart rate (*see the next subsection B*). We simulated these various hemodynamics, and searched for the condition to minimize minute LV oxygen consumption [2].

B. Hemodynamics

We used left ventricular (LV) end-systolic pressure-volume relationship (ESPVR) and the framework of ventricular-arterial coupling to reproduce hemodynamics [3]. We approximated LV ESPVR by a straight line, and coupled end-systolic elastance (E_{es}) with effective arterial elastance (E_a). E_a was approximated by R/T, where R was systemic vascular resistance and T was heart period, reciprocal of heart rate (HR).

Using these approximations, for a given LV end-diastolic stressed volume (V_{eds}), stroke volume (SV) and CO can be calculated as

$$SV = V_{eds} \frac{T \cdot E_{es}}{T \cdot E_{es} + R} \quad (1)$$

$$CO = V_{eds} \frac{E_{es}}{T \cdot E_{es} + R} \quad (2).$$

LV end-systolic stressed volume (V_{ess}) and pressure (P_{es})

978-1-4244-4122-8/11/$26.00 ©2011 IEEE

can be calculated as

$$V_{ess} = V_{eds} \frac{R}{T \cdot E_{es} + R} \quad (3)$$

$$P_{es} = V_{eds} \frac{E_{es} \cdot R}{T \cdot E_{es} + R} \quad (4).$$

In the framework of ventricular-arterial coupling, P_m was approximated by P_{es}. Systemic vascular resistance, R was therefore given by 1 mmHg·ml^{-1}·min·kg. Also, as P_{LA} was approximated by LV end-diastolic pressure (P_{ed}), V_{eds} would be calculated if we assume a predefined LV end-diastolic pressure-volume relationship (EDPVR). In this analysis, we used an exponential LV EDPVS as follows (V_{eds} in mL, P_{ed} in mmHg)

$$P_{ed} = \exp(0.082 \cdot V_{eds} - 0.8) + 2.03 \quad (5),$$

corresponding to the EDPVR with P_{ed} of 10 mmHg for V_{eds} of 35 ml.

Knowing R and V_{eds}, a necessary relationship between LV contractility (E_{es}) and heart period (T, an inverse of heart rate) is obtained. Even though it is necessary to follow this relationship to maintain P_m, CO, and P_{LA}, not a unique set of E_{es} and T would be obtained. Rather multiple sets of E_{es} and T would be feasible (*see the previous subsection A*).

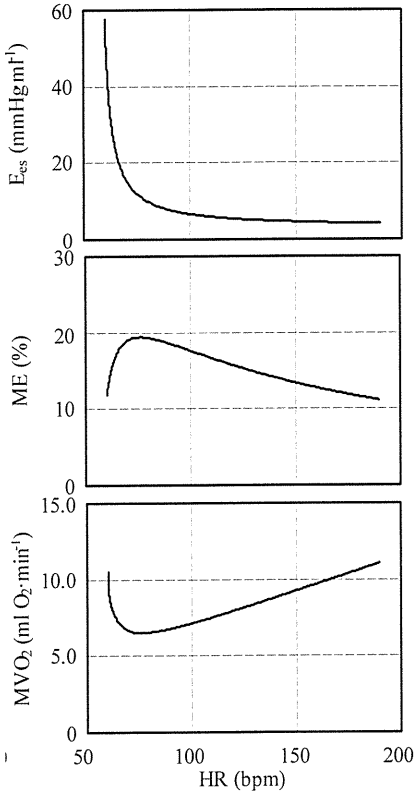

Fig. 1. Simulated relations of heart rate (HR) with left ventricular end-systolic elastance (E_{es}) (top), left ventricular mechanical efficiency (ME) (middle), and minute left ventricular oxygen consumption (MVO_2) (bottom), when mean blood pressure, cardiac output and left atrial pressure are kept at fixed values

C. Myocardial Oxygen Consumption

Beat LV oxygen consumption (BVO_2) was determined by PVA and E_{es} with high precision as follows [4]

$$BVO_2 = \alpha \cdot PVA + \beta \cdot E_{es} + \gamma \quad (6)$$

where α (1.8×10^{-5} mL O_2·mmHg^{-1}·mL^{-1}), β (1.8×10^{-3} mL O_2·mmHg^{-1}·mL), and γ (1.0×10^{-2} mL O_2) are constants. PVA stands for LV pressure-volume area (an index of total mechanical energy of LV contraction). PVA is the sum of LV stroke work (SW) and potential energy (PE). SW and PE are approximated as

$$SW = (P_m - P_{LA}) \cdot CO / HR \quad (7)$$

$$PE = P_{LA}^{\ 2} / 2E_{es} \quad (8).$$

Minute LV oxygen consumption per minute (MVO_2) and LV mechanical efficiency (ME) and are expressed as follows

$$MVO_2 = BVO_2 \cdot HR \quad (9)$$

$$ME = SW / BVO_2 = SW \cdot HR / MVO_2 \quad (10).$$

D. Simulation Results

Shown in Fig. 1 are simulation results. As explained in *subsection B*, there is an inverse relationship between E_{es} and heart rate [HR]. The top panel shows that if the heart is made bradycardiac, LV contractility should be enhanced to maintain P_m, CO, and P_{LA}, or to meet the peripheral demands.

The middle and the bottom panel show that ME would increase and MVO_2 would decrease by making heart bradycardiac up to a certain HR. Below this HR, however, rather ME would decrease and MVO_2 would increase with further decrease in HR. The differences in constants α, β and γ would change the optimal HR but would not change the basic relations show in Fig. 1.

E. Interpretation of the Simulation Results

As predicted by Eqs. 6 and 9, MVO_2 would largely be affected by HR. As MVO_2 is obtained by multiplying BVO_2 by HR, and as BVO_2 does not decrease much with HR, MVO_2 increases with HR.

In extreme bradycardiac condition, however, increase in E_{es} is so rapid, and the effect of increase in E_{es} overwhelmed the effect of HR.

ME is shown to be proportional to the reciprocal of MVO_2. Using, Eq. 7, the numerator of the right-hand side of Eq. 10, SW·HR is equal to (P_m-P_{LA})·CO and is constant.

III. Animal Experiment

We reproduced a similar condition as the previous simulation and examined if the same results would be obtained in an animal experiment [5].

A. Methods

We used 7 dogs for this animal experiment. These dogs were anesthetized and underwent coronary micro-embolization with glass beads. This procedure resulted in acute ischemic heart failure. We adjusted the size and the

dose of the emboli, so as to create heart failure severe enough that necessitated an intensive care. In these dogs, CO decreased by 39% (from 101±5 to 62±13 ml·min^{-1}·kg^{-1}), P_m decreased by 17 mmHg (from 114±4 to 97±14 mmHg), and P_{LA} increased by 8 mmHg (from 9 ± 1 to 17±2 mmHg).

To take the full control of HR in hand, a specific bradycardiac agent zatebradine (0.5 mg·kg^{-1}) was administered intravenously, and the intrinsic atrial beats were suppressed. Then, HR is fully controlled by atrial pacing. We first set HR at the rate before zatebradine infusion (146±8 bpm). In this condition (designated as *untreated*), we measured hemodynamics and cardiac energetics.

We then activated the autopilot system [1] we developed to maintain the desired P_m, CO, and P_{LA}. We customized in each animal the target values for P_m, CO, and P_{LA}. These ranged between 90 to 100 mmHg for P_m, 80 to 100 ml·min^{-1}·kg^{-1} for CO, and 10 to 12 mmHg for P_{LA}. The system restored P_m, CO and P_{LA} to their respective target values within 30 min. After confirming stable hemodynamics, (designated as *treated for hemodynamics*), we measured hemodynamics and cardiac energetics.

After the treatment of hemodynamics, we then reduced the atrial pacing rate in steps of 10 or 20 bpm. For each HR step, we waited until the hemodynamics stabilized. . We were able to reduce HR by 39±12 bpm. We measured hemodynamics and cardiac energetics at the lowest HR and stable hemodynamics (designated as *treated for hemodynamics and energetics*).

B. Results

We summarized the results of the animal experiment in Fig. 2. In each panel we plotted the pooled relationships between HR and various indexes of hemodynamics and cardiac energetics, in 7 dogs.

In *Untreated* condition (shown by open circles), CO was lower and P_{LA} was higher than normal. P_m was not so different from normal values. HR was quite high due to the activation of sympathetic nervous system.

By activating the autopilot system (*Treated for Hemodynamics* condition, shown by solid triangle), CO and P_{LA} were restored to the target normal values. P_m was slightly decreased. Because we are fully controlling HR, and we did not change the setting of HR, HR remained high also in this condition.

After decreasing HR to the lowest level (*Treated for Hemodynamics and Energetics* condition, shown by solid circle), all of CO, P_{LA}, and P_m remained the target normal values despite the large decrease in HR (CO: 89 ± 3 ml·min^{-1}·kg^{-1} to 88 ± 3 ml·min^{-1}·kg^{-1}, P_{LA}: 10.5 ± 0.4 mmHg to 10.9 ± 0.4 mmHg, P_m: 94 ± 3 mmHg to 93 ± 2 mmHg, all NS).

As shown in the right upper panel, the treatment for hemodynamics required the enhancement of contractility (E_{es}, $p<0.05$ vs. *Treated for Hemodynamics*); this is accomplished by the automatic infusion of a positive inotropic agent (dobutamine, increased from 1.4 ± 0.3 to 2.7 ± 0.5 μg·min^{-1}·kg^{-1}, $p<0.01$). With a decrease in heart rate, it is shown that a further increase in contractility was necessary to maintain CO, P_{LA}, and P_m. Doses for other drugs were also changed to maintain hemodynamics.

Although ME increased with the treatment for hemodynamics, this was at the expense of increasing MVO_2. With the treatment of hemodynamics and energetics, however, we were able to maintain hemodynamics, further improving ME ($p<0.01$ vs. *Treated for Hemodynamics*), and at the same time decreasing MVO_2 almost at the untreated level or rather to a lower level ($p<0.01$ vs. *Treated for Hemodynamics*). Even though we were unable to study extreme bradycardiac condition, a similar relationships were obtained as the theoretical analysis up to the heart rate studied (i.e., minimal heart rate was not below the optimal heart rate for minimizing myocardial oxygen consumption).

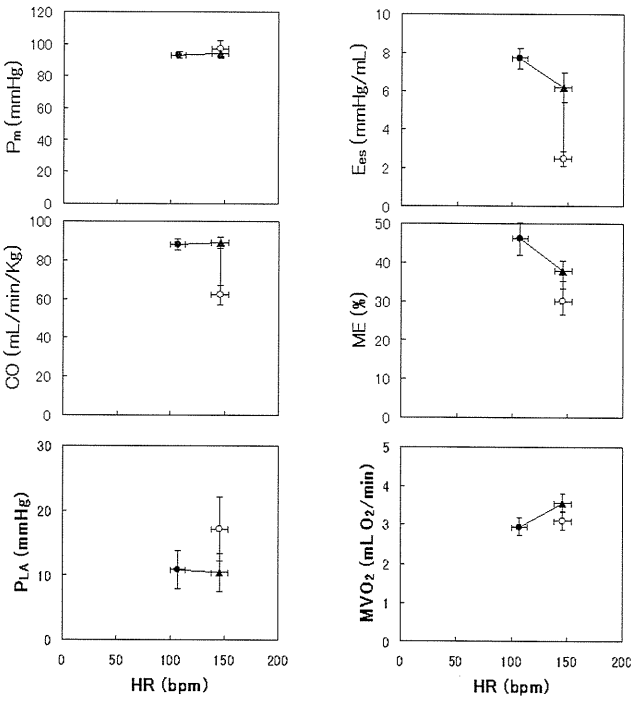

Fig. 2. Pooled relations between heart rate (HR) and mean blood pressure (P_m) (left top), cardiac output (CO) (left middle), left atrial pressure (P_{LA}) (left bottom), end-systolic elastance (E_{es}) (right top), left ventricular mechanical efficiency (ME) (right middle), and minute left ventricular oxygen consumption (MVO_2) (right bottom) in 7 dogs

IV. Conclusion

By taking full control of heart rate, and by adjusting treatment for hemodynamics at the same time, it was possible to maintain hemodynamics without sacrificing LV oxygen consumption.

REFERENCES

[1] K. Uemura, A. Kamiya, I. Hidaka, T. Kawada, S. Shimizu, *et al.*, "Automated drug delivery system to control systemic arterial pressure, cardiac output, and left heart filling pressure in acute decompensated heart failure," *J. Appl. Physiol.* vol. 100, no 4, 1278-1286, Apr. 2006.

[2] M. Sugimachi, K. Todaka, K. Sunagawa, M. Nakamura, "Optimal afterload for the heart vs. optimal heart for the afterload," *Front. Med. Biol. Eng.* vol. 2, no. 3, 217-221, 1990.

[3] K. Sunagawa, K. Sagawa, W. L. Maughan, "Ventricular interaction with the loading system," *Ann. Biomed. Eng.* vol. 12, no. 2, 163-189, 1984.

[4] H. Suga, "Ventricular energetics," *Physiol. Rev.* vol. 70, no. 2, 247-277, Apr. 1990.

[5] K. Uemura, K. Sunagawa, M. Sugimachi, "Computationally managed bradycardia improved cardiac energetics while restoring normal hemodynamics in heart failure," *Ann. Biomed. Eng.* vol. 37, no. 1, 82-93, Jan. 2009.

33rd Annual International Conference of the IEEE EMBS
Boston, Massachusetts USA, August 30 - September 3, 2011

Impact of baroreflex on venous return surface

Takafumi Sakamoto, Yoshinori Murayama, Atsushi Tanaka, Kazuo Sakamoto, Tomoyuki Tobushi, Keita Saku, Kazuya Hosokawa, Ken Onitsuka, Takeo Fujino and Kenji Sunagawa, Senior *Member, IEEE*

Abstract— **Background: Although Guyton's concept of venous return (VR) revolutionized circulatory physiology, the pulmonary circulation is invisible in its original framework. Since the pulmonary circulation is critical in left heart failure, we characterized the VR as a surface described by right (P_{RA}) and left atrial (P_{LA}) pressures and demonstrated that the VR surface was capable of representing mechanics of pulmonary as well as systemic circulation. However how baroreflex impacts the VR surface remains unknown. Methods/Results: In 8 dogs, we isolated the carotid sinuses and replaced both ventricles with pumps. We varied cardiac output, shifted blood distribution between the systemic and pulmonary circulation at carotid sinus pressures (CSP) of 100 or 140 mmHg. The coefficient of determination of the VR surface ranged 0.96-0.99 indicating how flat the surface is. Increasing CSP decreased maximum VR (233±27 vs. 216±33 ml/kg/min, p<0.05), whereas did not change the slopes of VR along P_{RA} or P_{LA} axes. Conclusions: Baroreflex parallel shifts the VR surface, thereby stressed volume, without changing its slopes.**

I. Introduction

Guyton's classic concept of circulatory equilibrium [1] revolutionized circulatory physiology. Guyton's classic concept, however, was not intended to represent the circulatory equilibrium of left ventricular failure because neither left ventricular mechanics nor pulmonary circulation is explicitly incorporated. To overcome such a limitation of Guyton's classic concept, we previously developed a framework of circulatory equilibrium [2, 3] where, as shown in Fig. 1, we defined the cardiac output curve and venous return curve as functions of both right atrial pressure (P_{RA}) and left atrial pressure (P_{LA}). We denoted the venous return curve as the venous return surface. A theoretical analysis using a distributed vascular model indicated that venous return (VR) of the total circulatory system can be described as

$$VR=VR_{max}-(G_P P_{LA}+G_S P_{RA}) \qquad (1)$$

where VR_{max} is maximum venous return and is a function of stressed blood volume [2, 3, 4], G_P and G_S, conductance of pulmonary and systemic venous return, respectively. We demonstrated that the venous return surface was remarkably flat and the slopes toward the P_{LA} and P_{RA} axes did not differ among animal preparations [2, 3].

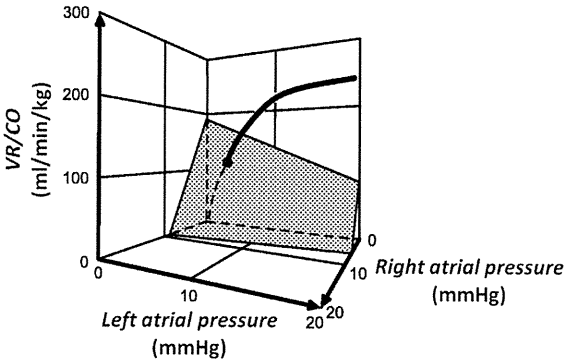

Figure 1 Proposed framework of circulatory equilibrium consists of integrated cardiac output curve and venous return surface.

Since baroreflex is a powerful physiological modulator of mechanical properties of cardiovascular system and thereby capable of changing circulatory equilibrium, we investigated how baroreflex impacts on characteristics of venous return surface.

II. Methods

A. Animal preparation

Eight mongrel dogs were anesthetized with pentobarbital sodium and ventilated artificially. We isolated the bilateral carotid sinuses from the systemic circulation and connected them to a servo-controlled piston pump to control intra-carotid sinus pressure (CSP). We cut the bilateral vagosympathetic trunks to eliminate other reflexes. After median sternotomy, the heart was suspended in a pericardial cradle. Fluid-filled catheters were placed in the right and left atrium to measure pressures.

To examine the venous return surface, we performed total heart bypass. Two roller pumps were used to control systemic and pulmonary flows. A systemic perfusion cannula was placed in the right common carotid artery. A draining cannula for the systemic circulation was inserted into the right ventricle through its free wall. A pulmonary perfusion cannula was placed in the pulmonary artery. A draining cannula for pulmonary circulation was inserted into the left ventricle via the apex. The flow rate (i.e., cardiac output) was measured by an in-line ultrasonic flow probe. After starting two roller pumps at a matched rate, we tied an umbilical tape around pulmonary artery, clamped the ascending aorta and thus established the total heart bypass.

B. Protocol

For a given CSP, we waited for several minutes until the

Manuscript received September 15, 2011. This work was supported in part by Health and Labour Sciences Research Grant for Research on Medical Devices for Improving Impaired QOL from the Ministry of Health Labour and Welfare of Japan, Health and Labour Sciences Research Grant for Clinical Research from the Ministry of Health Labour and Welfare of Japan, and Grant-in-Aid for Scientific Research(S) (18100006) from the Japan Society for the Promotion of Science

All authors are with Kyushu University, Fukuoka 8128582 Japan. (corresponding author Takafumi Sakamoto to provide phone: +81-92-642-5360; fax: +81-92-642-5357; e-mail: tsaka@cardiol.med.kyushu-u.ac.jp).

hemodynamic conditions reached a steady state. We then simultaneously changed the flow rate of both pumps stepwise between 40 and 100 ml/min/kg in an increment of 20ml /min/kg. In each step, we varied the blood volume distribution between the pulmonary and the systemic circulations by transiently unbalancing the flow rates of the two pumps. We conducted the protocol at CSP of 100 and 140 mmHg.

III. Results

We applied multivariate regression analysis and determined VR_{max}, G_P and G_S. Shown in the left panel of Fig. 2 is a representative venous return surface. All data points appear to be distributed on a flat surface. The fact that all points are distributed around a single line if they are viewed from a direction parallel to the surface indicated how flat the surface is (not shown). Baroreflex did not affect the flatness of the venous return surface. The multiple correlation coefficient was close to unity (r2=0.96-0.99) suggesting that the venous return surface is reasonably flat in every animal.

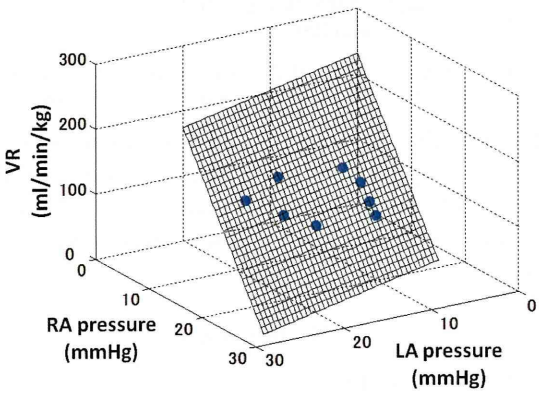

Figure 2 Representative venous return surface at CSP 140mmHg

Illustrated in Fig. 3 are the impact of baroreflex on VR_{max}, G_S and G_P. Increasing CSP significantly decreased VR_{max}, (233±27 vs. 216±33 ml/kg/min, data were means ± SD, $p<0.05$, paired t-test) whereas it did not change G_P or G_S. This is to say that baroreflex shifted the VR surface along the vertical axis without changing the slopes. Since the VR_{max} reflects stressed blood volume [2, 3], baroreflex in turn changed stressed blood volume.

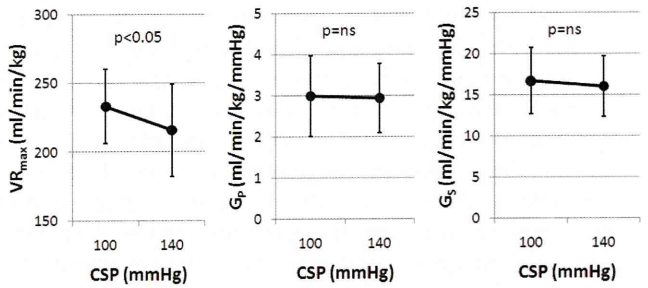

Figure 3 VR_{max}, G_P, *and* G_S obtained at CSP 100 and 140 mmHg

IV. Discussion

Uemura et al [2, 3] have demonstrated that VR surface was remarkably flat and the slopes toward P_{LA} and P_{RA} axes did not differ among animal preparations. But the impact of baroreflex on VR surface remained unknown. We reconfirmed that the venous return surface is reasonably flat over a wide range of cardiac output and venous pressures. Baroreflex did not affect the flatness of the venous return surface. Baroreflex markedly changes the maximum venous return, thereby stressed volume, but did not change the slopes of the venous return surface.

V. Conclusion

We conclude that baroreflex modulates the circulatory equilibrium by changing the stressed blood volume without affecting the slopes of venous return.

Acknowledgment

This study was supported in part by Health and Labour Sciences Research Grant for Research on Medical Devices for Improving Impaired QOL from the Ministry of Health Labour and Welfare of Japan, Health and Labour Sciences Research Grant for Clinical Research from the Ministry of Health Labour and Welfare of Japan, Grant-in-Aid for Scientific Research(S) (18100006, 23220013) from the Japan Society for the Promotion of Science.

References

[1] A.C. Guyton, "Textbook of Medical Physiology", *1956.*

[2] K. Uemura, M. Sugimachi, T. Kawada, A. Kamiya, Y. Jin, K. Kashihara, and K. Sunagawa, "A novel framework of circulatory equilibrium," *Am J Physiol Heart Circ Physiol 286: H2376-H2385, 2004.*

[3] K. Uemura, T. Kawada, A. Kamiya, T. Aiba, I. Hidaka, K. Sunagawa, and M. Sugimachi, "Prediction of circulatory equilibrium in response to changes in stressed blood volume," *Am J Physiol Heart Circ Physiol 289: H301-H307, 2005.*

[4] K. Sagawa, L. Maughan, H. Suga, K. Sunagawa, "Cardiac Contraction and Pressure-Volume Relationship," *Oxford Univ. Press, p. 232-298, 1988.*

33rd Annual International Conference of the IEEE EMBS
Boston, Massachusetts USA, August 30 - September 3, 2011

Experimental 'Jet Lag' Causes Sympathoexcitation via Oxidative Stress through AT_1 Receptor in the Brainstem

T. Kishi, K. Sunagawa

***Abstract*- Circadian disruptions through frequent transmeridian travel, rotating shift work, and poor sleep hygiene are associated with an array of physical and mental health maladies, including the abnormal autonomic nervous system. We have demonstrated that the oxidative stress through AT_1 receptor in the brain activates sympathetic nervous system. The aim of the present study was to determine whether experimental 'jet lag' causes sympathoexcitation via oxidative stress through AT_1 receptor in the cardiovascular center of the brainstem (rostral ventrolateral medulla; RVLM) or not. Experimental 'jet lag' was made to normotensive (Wister-Kyoto rat; WKY rat) and hypertensive rats (stroke-prone spontaneously hypertensive rats; SHRSP) by the exposure to a 12 hour phase advance for 5 days. In WKY, 'jet lag' increases blood pressure and the activity of sympathetic nervous system via oxidative stress through angiotensin II type 1 receptor in the RVLM for 2 days only, and the changes are improved at 3 day after the initiation of 'jet lag'. In SHRSP, 'jet lag' also increases blood pressure and the activity of sympathetic nervous system via oxidative stress through angiotensin II type 1 receptor in the RVLM, and the changes are greater compared to those in WKY, and are maintained for the period of 'jet lag'. These results suggest that experimental 'jet lag' causes sympathoexcitation via oxidative stress through AT_1 receptor in the brain, especially in hypertension.**

INTRODUCTION

Frequent transmeridian travel is known to cause an disturbance in circadian timing system [1, 2]. This disturbance is associated with a number of clinical pathologies, including a higher incidence of hypertension and cardiovascular disease [3, 4]. In mammals, the master circadian pacemaker is located in the suprachiasmatic nucleus (SCN) in the anterior hypothalamus, and the SCN generates endogenous oscillations with a period of approximately 24 hours [5]. At the cellular level, circadian rhythms are generated by 24-hour autoregulatory transcriptional feedback loops consisting of 'clock' genes and their protein products [6]. A recent study suggests that the circadian disruption lead to marked suppression of hippocampal cell proliferation and neurogenesis, associated with notable deficits in learning and memory [7].These results indicate that 'jet lag' causes the changes in neural structures and functions in the brain. In terms of the regulation of blood pressure and heart rate via sympathetic nervous system, central nervous system involved in baroreflex circuit is important [8]. However, it has not been determined whether the abnormalities in blood pressure and heart rate in 'jet lag' are due to the changes in central nervous system or not.

We have demonstrated that nitric oxide and oxidative stress in the brainstem regulates the activity of the sympathetic nervous system [9, 10]. Especially, in the brainstem, oxidative stress through the angiotensin II type 1 receptor in the rostral ventrolateral medulla (RVLM) causes the sympatho-excitation [11]-[13]. Taken together, we hypothesize that 'jet lag' might cause hypertension through the sympathoexcitation due to the oxidative stress in the RVLM. However, the mechanisms in which 'jet lag' causes hypertension or sympathoexcitation have not been fully determined.

The aims of the present study was to determine whether the experimental 'jet lag' causes sympathoexcitation or not, and if so, whether the experimental 'jet lag'-induced sympathoexcitation is due to the oxidative stress through AT_1 receptor in the RVLM or not. To do these aims, we made the experimental 'jet lag' model rats by the exposure to a 12 hour phase advance for 5 days.

PROCEDURES

Ethics statement

This study was reviewed and approved by the committee on ethics of Animal Experiments, Kyushu University Graduate School of Medical Sciences, and conducted according to the Guidelines for Animal Experiments of Kyushu University.

Animals

Adult male stroke-prone spontaneously hypertensive rats (SHRSP) and Wister-kyoto (WKY) rats maintained on a 14:10 light:dark (LD) cycle (Lights on at 0700 h) prior to the onset of the experiments, with a light

Manuscript submitted April 15, 2011, revised manuscript submitted June 20, 2011.

T. Kishi is with the Department of Advanced Therapeutics for Cardiovascular Diseases, Kyushu University Graduate School of Medical Sciences, Fukuoka, 812-8582 Japan (phone: +81-92-642-5360; fax: +81-92-642-5374; e-mail: tkishi@cardiol.med.kyushu-u.ac.jp).

intensity ranging from 100-300 lux at the level of each cage. All animals were maintained in a colony room and provided with ad libitum access to water and food.

Experimental 'Jet Lag'

WKY and SHRSP were divided into two groups, 'jet lag'-WKY, control-WKY, 'jet lag'-SHRSP, and control-SHRSP. 'Jet lag'-WKY and –SHRSP groups were exposed to a 12 hour phase advance for 5 days, while control-WKY and –SHRSP groups were remained in a 14:10 LD (lights on at 0700 hr) cycle for the same duration.

Measurement of Blood Pressure and Heart rate

The UA-10 telemetry system (Data Sciences International) was used to measure mean arterial pressure and heart rate. The surgical procedure has been described previously [9, 11]. Mean arterial pressure and heart rate were recorded continuously for 10 minutes every day in light and dark phase by a multichannel amplifier and signal converter.

Urinary Norepinephrine Excretion As an Parameter of the Activity of Sympathetic Nervous System

As the parameter of the activity of the sympathetic nervous, we measured the urinary norepinephrine concentration by high-performance liquid chromatography (HPLC), and calculated the urinary norepinephrine excretion for 24 hours [9]-[13].

Oxidative Stress in the RVLM

As an indicator of the oxidative stress in the RVLM, we measured thiobarbituric acid-reactive substances (TBARS) levels in the tissues obtained from the RVLM of each group at the end of the study as described in previous studies [11]-[13]. Moreover, to determine the TBARS levels in the RVLM at 2 day after the initiation of 'jet lag', we made the other 4 groups, 'jet lag' for 2 days-WKY, control-WKY, 'jet lag' for 2 days-SHRSP, and control-SHRSP.

Microinjection of Angiotensin II Type 1 Receptor Blocker into the RVLM

To inhibit the angiotensin II type 1 receptor in the RVLM locally, we microinjected losartan (1nmol), angiotensin II type 1 receptor blocker, into the bilateral RVLM of each group at the end of the study. Moreover, to determine the activity of the angiotensin II type 1 receptor in the RVLM at 2 day after the initiation of 'jet lag', we made the other 4 groups, 'jet lag' for 2 days-WKY, control-WKY, 'jet lag' for 2 days-SHRSP, and control-SHRSP. Each rat was anesthetized with sodium pentobarbital. A catheter was inserted into the femoral artery to record arterial blood pressure. A tracheal cannula was connected to a ventilator, and the rats were artificially ventilated. The rats were placed in a stereotaxic frame. The identification of the RVLM and the procedures of the microinjection were confirmed as described previously [11]-[13].

RESULTS

Blood Pressure and Heart rate

Fig.1 shows the results of mean arterial pressure. Prior to the experiments, mean arterial pressure and heart rate were significantly higher in SHRSP than in WKY both at light and dark phase (Fig. 1 and 2). For the rats, light phase is a rest phase, and dark phase is an active phase. In dark and light phase, mean arterial pressure and heart rate were significantly higher in 'jet lag'-WKY than in control-WKY at 1-2 day after the initiation of 'jet lag', and was similar in 'jet lag'-WKY and control-WKY at 3-5 day after the initiation of 'jet lag' (Fig. 1 and 2). In dark phase, mean arterial pressure and heart rate were similar in 'jet lag'-SHRSP and control-SHRSP (Fig. 1 and 2). However, in light phase, mean arterial pressure and heart rate were significantly higher in 'jet-lag'-SHRSP than in control-SHRSP for the 'jet lag' period (Fig. 1 and 2).

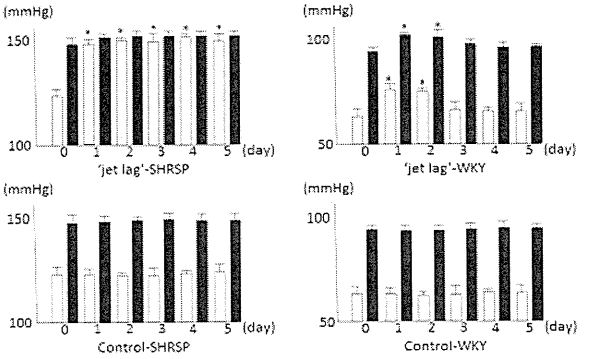

Fig 1. The results of mean arterial pressure in each group. White column indicates light phase, and black column indicates dark phase. N=5 for each. *P<0.05 vs control.

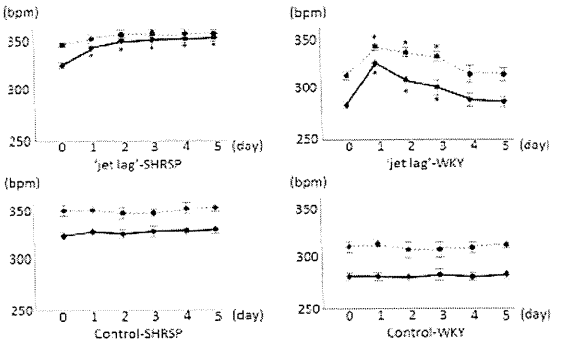

Fig 2. The results of the averages of heart rate in each group. Solid line indicates light phase, and dot line indicates dark phase. N=5 for each. *P<0.05 vs control.

Urinary Norepinephrine Excretion

Prior to the experiments, urinary norepinephrine excretion was significantly higher in SHRSP than in WKY (Fig. 3). In WKY, urinary norepinephrine excretion was significantly higher in 'jet lag'-WKY than in control-WKY at 1-2 day after the initiation of 'jet lag', and was similar in 'jet lag'-WKY and control-WKY at 3-5 day after the initiation of 'jet lag' (Fig. 3). In SHRSP, urinary Units norepinephrine excretion was significantly higher in 'jet lag'-SHRSP than in control-WKY for the period of 'jet lag' (Fig. 3).

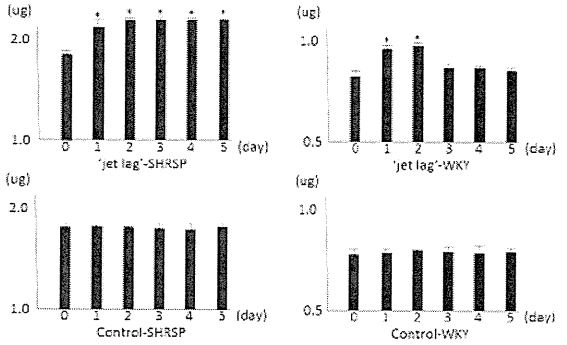

Fig 3. The results of the urinary norepinephrine excretion in each group for 5 days of jet lag. N=5 for each. *P<0.05 vs control.

Oxidative Stress in the RVLM

In WKY, TBARS in the RVLM was significantly higher in 'jet lag'-WKY than in control-WKY at 2 day after the initiation of 'jet lag', and was similar in 'jet lag'-WKY and control-WKY at 5 day after the initiation of 'jet lag' (Fig. 4). In SHRSP, TBARS in the RVLM was significantly higher in 'jet lag'-SHRSP than in control-WKY both at 2 and 5 day after the initiation of 'jet lag' (Fig. 4).

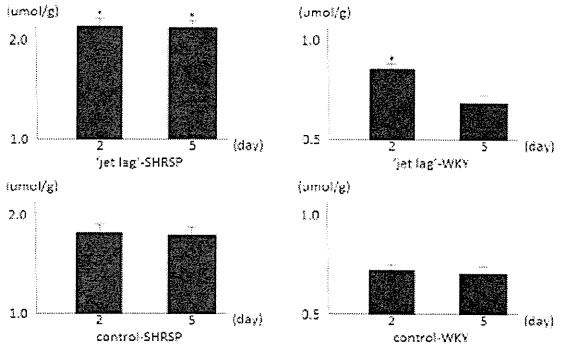

Fig 4. The results of the levels of TBARS in the RVLM of each group. N=5 for each. *P<0.05 vs control.

Microinjection of Angiotensin II Type 1 Receptor Blocker into the RVLM

In WKY, the depressor effect due to the microinjection of losartan into the RVLM was significantly greater in 'jet lag'-WKY than in control-WKY at 2 day after the initiation of 'jet lag', and was similar in 'jet lag'-WKY and control-WKY at 5 day after the initiation of 'jet lag' (Fig. 5). In SHRSP, the depressor effect was significantly greater in 'jet lag'-SHRSP than in control-WKY both at 2 and 5 day after the initiation of 'jet lag' (Fig. 5).

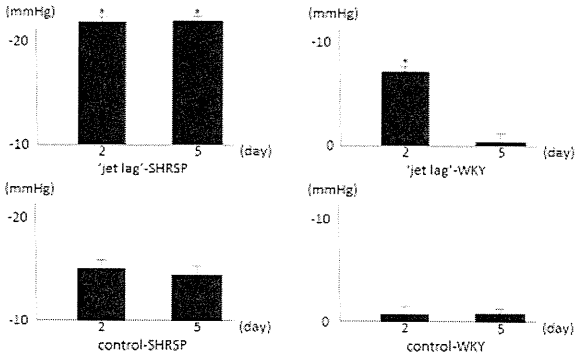

Fig 5. The results of the degree of the depressor effects due to the microinjection of losartan into the RVLM. N=5 for each. *P<0.05 vs control.

DISCUSSION

In the present study, we demonstrated that 1) in WKY, 'jet lag' increases blood pressure and the activity of sympathetic nervous system via oxidative stress through angiotensin II type 1 receptor in the RVLM for 2 days only, and the changes are improved at 3 day after the initiation of 'jet lag', 2) in SHRSP, 'jet lag' also increases blood pressure and the activity of sympathetic nervous system via oxidative stress through angiotensin II type 1 receptor in the RVLM, and the changes are maintained for the period of 'jet lag'. From these results, we consider that 'jet lag' causes sympathoexcitation via oxidative stress through angiotensin II type 1 receptor in the RVLM, and the 'jet lag'-induced sympathoexcitation is maintained and excessive in SHRSP. The clinical implications from the present study are that hypertension is a risk of 'jet lag'-induced sympathoexcitation, and that angiotensin II type 1 receptor blocker might be an effective agent of the treatment for 'jet lag'-induced sympathoexcitation.

The most important finding in the present study is that 'jet lag' activates the angiotensin II type 1 receptor in the brain. The activity of the sympathetic nervous system is regulated mainly by the angiotensin II type 1 receptor-induced oxidative stress in the RVLM [11]-[13]. Previous studies have suggested that 'jet lag' increases blood pressure [3]-[4]. Taken together, we consider that the mechanisms of 'jet lag'-induced hypertension and sympathetic activation might be due to the activation of the angiotensin II type 1 receptor in the brain. Furthermore, while the sympathoexcitation is tentative in WKY, the sympathoexcitation is maintained in SHRSP. We should consider that hypertension is a worsening factor of 'jet lag'-induced sympathoexcitation.

In terms of the treatment for 'jet lag'-induced sympathoexcitation, the target of the treatment might be angiotensin II type 1 receptor in the RVLM. To inhibit the angiotensin II type 1 receptor in the brain, in the present study, we performed the microinjection of the angiotensin II type 1 receptor blocker directly into the RVLM, and in our previous study, we performed the intracerebroventricular infusion of the angiotensin II type 1 receptor blocker [13]. In clinical aspects, oral administration of angiotensin II type 1 receptor blocker might be a novel agent, because some oral intake of angiotensin II type 1 receptor blocker affects the RVLM through the blood-brain barrier [10]. Moreover, we have also demonstrated that some other oral agents, especially statin, have the potential to inhibit the oxidative stress in the brain [10, 14]. In the further study, we should examine the effects of the oral administration of the angiotensin II type 1 receptor blocker s and / or statins on the 'jet lag'-induced sympathoexcitation.

The mechanisms in which 'jet lag' activates the angiotensin II type 1 receptor in the brain have not been determined in the present study. In hypertension, previous studies have suggested that the angiotensin II type 1 receptor in the brain is activated by the circulating angiotensin II and / or baroreflex circuit [8, 10]. In the present study, we did not determine the changes in the concentration of plasma angiotensin II and the baroreflex sensitivity. Further studies must be done to determine mechanisms in which 'jet lag' activates the angiotensin II type 1 receptor in the brain.

There are some limitations in the present study. First, we only examined the oxidative stress in the RVLM. The increase in oxidative stress in the brain of 'jet lag' may not be the unique phenomenon in the RVLM. However, in the regulation of sympathetic nerve activity, RVLM is the most important cite. Furthermore, in the RVLM, oxidative stress is the most powerful and important sympatho-exciting factor [11, 13]. From these reasons, we focused on the oxidative stress in the RVLM. Second, we did not perform the long-term RVLM-specific inhibition of AT_1 receptor. We must do the RVLM-specific knock down of AT_1 receptor in the future study.

CONCLUSION

The results from the present study suggest that experimental 'jet lag' causes sympathoexcitation via oxidative stress through AT_1 receptor in the brain, especially in hypertensive states.

APPENDIX

None.

ACKNOWLEDGEMENT

This work was supported by a Grant-in-Aid for Scientific Research from the Japan Society for the Promotion of Science (B193290231).

REFERENCES

[1] A.J. Davidson, O. C. Castanon, T. L. Leise, P. C. Molyneux, M. E. Harrington, "Visualizing jet lag in the mouse suprachiasmatic nucleus and peripheral circadian timing system", Eur J Neurosci, vol. 29, pp. 171-180, 2009.

[2] E. S. Maywood, J. O'Neill, G. K. Wong, A. B. Reddy, M. H. Hastings, "Circadian timing in health and disease", Prog Brain Res, vol. 153, pp. 253-269, 2006.

[3] M. Ha, J. Park, "Shiftwork and metabolic risk factors of cardiovascular disease", J Occup Health, vol. 47, pp. 89-95, 2005.

[4] M. Kivimaki, M. Virtanen, M. Elovainio, A. Vaananen, L. K. Jarvinen L, "Prevalent cardiovascular disease, risk factors and selection out of shift work", Scand J Work Environ Health, vol. 32, pp. 204-208, 2006.

[5] R. Y. Moore, V. B. Eichker, "Loss of a circadian adrenal corticosterone rhythm following suprachiasmatic lesions in the rat", Brain Res, vol. 42, pp. 201-206, 1972.

[6] R. Chen, A. Schirmer, Y. Lee, H. Lee, V. Kumar, "Rhythmic PER abundance defines a critical nodal point for negative feedback within the circadian clock mechanisms", Mol Cell, vol. 36, pp. 417-430, 2009.

[7] E. M. Gibson, C Wang, S Tjho, N Khattar, L.J. Kriegsfeld, "Experimental 'jet lag' inhibits adult neurogenesis and produces long-term cognitive deficits in female hamsters", PloS ONE, vol. 5, e15267, 2010.

[8] P. G. Guyenet PG, "The sympathetic control of blood pressure", Nat Rev Neurosci, vol. 7. pp. 335-346, 2006.

[9] Y. Hirooka, K. Sakai, T. Kishi, A. Takeshita, "Adenovirus-mediated gene transfer into the NTS in conscious rats: A new approach to examining the central control of cardiovascular regulation", Ann N Y Acad Sci, vol. 940, pp. 197-205, 2001.

[10] Y. Hirooka, T. Kishi, K. Sakai, A. Takeshita, K. Sunagawa, "Imbalance of central nitric oxide and reactive oxygen species in the regulation of sympathetic activity and neural mechanisms of hypertension", Am J Physiol, vol. 300, pp. R818-R826, 2011.

[11] T. Kishi, Y. Hirooka, Y. Kimura, K. Ito, H. Shimokawa, A. Takeshita, "Increased reactive oxygen species in rostral ventrolateral medulla contribute to neural mechanisms of hypertension in stroke-prone spontaneously hypertensive rats", Circulation, vol. 109, pp. 2357-2362, 2004.

[12] M. Nozoe, Y. Hirooka, Y. Koga, S. Araki, S. Konno, T. Kishi, T. Ide, K. Sunagawa K, "Mitochondria-derived reactive oxygen species mediate sympathoexcitation induced by angiotensin II in the rostral ventrolateral medulla", J Hypertens, vol. 26, pp. 2176-2184, 2008.

[13] T. Kishi, Y. Hirooka, S. Konno, K. Ogawa, K. Sunagawa, "Angiotensin II type 1 receptor-activated caspase-3 through ras/mitgen-activated protein kinase-extracellular signal-regulated kinase in the rostral ventrolateral medulla is involved in sympathoexcitation in stroke-prone spontaneously hypertensive rats", Hypertension, vol. 55, pp. 291-294, 2010.

[14] T. Kishi, Y. Hirooka, H. Shimokawa, A. Takeshita, K. Sunagawa, "Atorvastatin reduces oxidative stress in the rostral ventrolateral medulla of stroke-prone spontaneously hypertensive rats", Clin Exp Hypertens, vol. 30, pp. 1-9, 2008.

33rd Annual International Conference of the IEEE EMBS
Boston, Massachusetts USA, August 30 - September 3, 2011

Artificial Baroreflex System Restores Volume Tolerance in the Absence of Native Baroreflex

Kazuya Hosokawa, Kouta Funakoshi, Atsushi Tanaka, Takafumi Sakamoto, Ken Onitsuka, Kazuo Sakamoto, Tomoyuki Tobushi, Takeo Fujino, Keita Saku, Yoshinori Murayama, Tomomi Ide and Kenji Sunagawa, *Senior Member, IEEE*

Abstract— **The arterial baroreflex stabilizes arterial pressure by modulating the mechanical properties of cardiovascular system. We previously demonstrated that the baroreflex impairment makes the circulatory system extremely sensitive to volume overload and predisposes to pulmonary edema irrespective of left ventricular systolic function. To overcome the volume intolerance, we developed an artificial baroreflex system by directly stimulating the carotid sinus nerves in response to changes in arterial pressure. The artificial baroreflex system precisely reproduced the native arterial pressure response and restored physiological volume buffering function. We conclude that the artificial baroreflex system would be an attractive tool in preventing pulmonary edema in patients with impaired baroreflex function.**

I. Introduction

Heart failure is a major medical problem worldwide. Although latest therapeutic strategy benefits many patients with heart failure, their prognosis remains unacceptably poor [1]. We demonstrated that baroreflex failure induces volume intolerance and predisposes to pulmonary edema irrespective of left ventricular systolic function. At present, no therapeutic strategy to restore baroreflex function is available. The aim of this study is to develop an artificial baroreflex system capable of restoring volume buffering function.

Manuscript received April 15, 2011. This work was supported in part by Health and Labour Sciences Research Grant for Research on Medical Devices for Improving Impaired QOL from the Ministry of Health Labour and Welfare of Japan, Health and Labour Sciences Research Grant for Clinical Research from the Ministry of Health Labour and Welfare of Japan, and Grant-in-Aid for Scientific Research(S) (18100006) from the Japan Society for the Promotion of Science

Authors are with Kyushu University Graduate School of Medical Sciences, Department of Cardiovascular Medicine. 8128582 Higashi-ku, Maidashi 3-1-1, Fukuoka, Japan (corresponding author K. Hosokawa to provide phone: +81-92-642-5360; fax: +81-92-642-5357; e-mail: ncvchoso@cardiol.med.kyushu-u.ac.jp).

II. Methods

Surgical Preparations

The care and use of the animals were strict accordance with the guiding principles of our institution. In 14 anesthetized Sprague-Dawley rats weighing 562±37g, the baroreceptor regions were vascularily isolated [2]. The intra-carotid sinus pressure (CSP) was controlled by a servo-controlled piston pump (ET-126A and PA-119; Labworks, Costa Mesa, CA). Bilateral aortic depressor nerves were cut and a pair of electrodes was attached to the proximal end of the aortic depressor nerves for stimulation.

Framework of the artificial baroreflex system

As shown in Fig. 1, the artificial baroreflex system consisted of a pressure sensor, regulator and neuro-stimulator. The operating rule (H_{ABS}), how the regulator translates arterial pressure (AP) into stimulation (STM), was identified by the ratio of transfer functions from CSP to AP ($H_{CSP\text{-}AP}$) to that from STM to AP ($H_{STM\text{-}AP}$). To obtain $H_{CSP\text{-}AP}$ and $H_{STM\text{-}AP}$, we perturbed CSP and the pulse frequency of the neuro-stimulation with random binary sequences (Data were not shown).

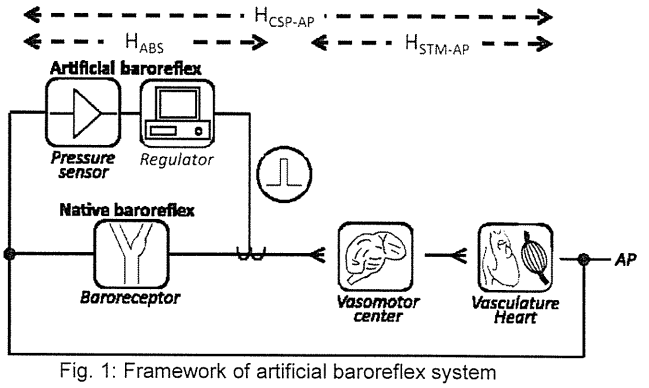

Fig. 1: Framework of artificial baroreflex system

A. Protocol-1: Comparison of open-loop pressure regulation between the native baroreflex and artificial baroreflex system

We implemented identified H_{ABS} into the regulator. Under the open loop condition (Fig. 2), we alternatively imposed pressure changes stepwise into CSP and the pressure sensor of the artificial baroreflex system. We then compared the arterial pressure responses.

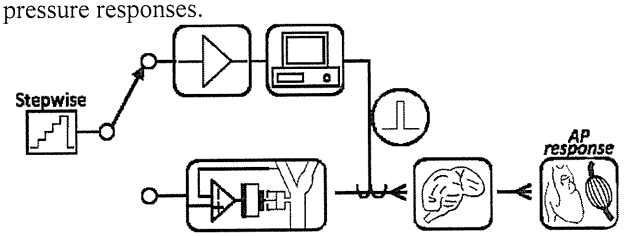

Fig. 2: Comparison of open-loop pressure regulation between the native baroreflex and artificial baroreflex system (Protocol -1)

B. Protocol-2: Comparison of volume buffering function between the native baroreflex and artificial baroreflex system

Under the closed loop condition of the native or artificial baroreflex system (Fig. 3), in order to examine the volume buffering function, we infused dextran stepwise and measured left atrial pressure (LAP) every 1 minute until LAP reaches 11mmHg. We plotted the LAP-infused volume relationships.

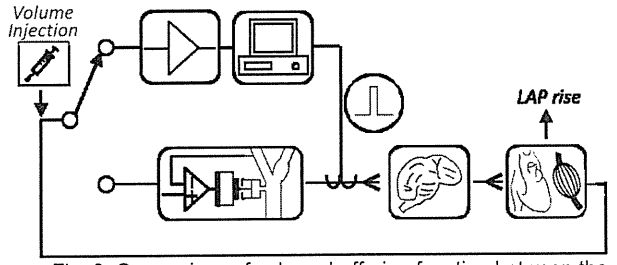

Fig. 3: Comparison of volume buffering function between the native baroreflex and artificial baroreflex system (Protocol-2)

III. Results

Identification of the H_{ABS}

Both H_{CSP-AP} and H_{STM-AP} showed the characteristics of lowpass filter with similar corner frequencies. Taking the ratio of H_{CSP-AP} to H_{STM-AP} yielded H_{ABS} (Data were not shown).

A. Protocol-1: Comparison of open-loop pressure regulation between the native baroreflex and artificial baroreflex system

The arterial pressure responses between the native baroreflex and artificial baroreflex system were indistinguishable (Fig. 4). Maximal gain was -2.28±0.88 in the native baroreflex and was -2.20±1.18 (NS, n=7) in the artificial baroreflex system.

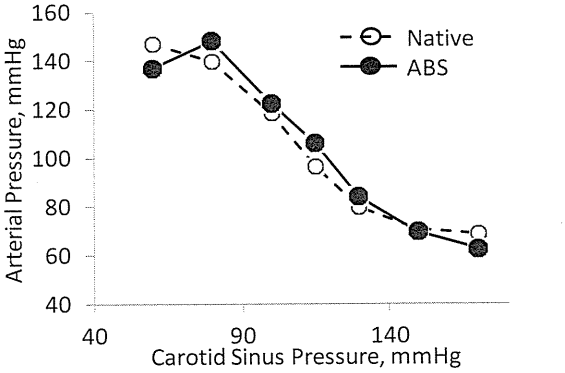

Fig. 4: The artificial baroreflex system reproduces the native baroreflex function

B. Protocol-2: Comparison of volume buffering function between the native baroreflex and artificial baroreflex system

In comparison with no baroreflex, the native baroreflex markedly buffered the increase in LAP in response to volume infusion. The artificial baroreflex system was as powerful as the native baroreflex in buffering the increase in LAP to volume infusion (Fig. 5).

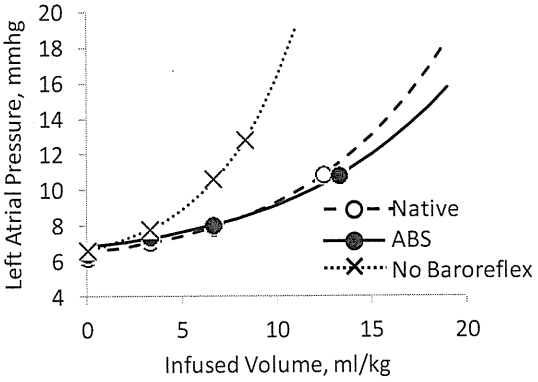

Fig. 5: The artificial baroreflex system restores normal volume buffering function

IV. Discussion

We have shown that the artificial baroreflex system reproduced the open-loop characteristics of baroreflex pressure regulation reasonably well including the saturation and threshold effects of native baroreflex (Fig. 4). Since electrical stimulation of the carotid sinus nerves is linearly dependent on input arterial pressure (CSP), the reproduction of the nonlinear pressure responses would like to reflect the nonlinear sympathetic activation by the central mechanism.

The artificial baroreflex system restored physiological volume buffering function (Fig. 5). We estimated the amount of volume required to induce pulmonary edema by fitting the LAP-infused volume relationship to a monoexponential curve. We defined the critical volume load (critical ΔV) at which LAP reaches 18mmHg. The critical volume was 21.0±3.0ml/kg in the artificial baroreflex system and 20.1±3.0ml/kg in the native baroreflex, compared with 16.6 ± 4.4ml/kg in no baroreflex. The critical ΔV was markedly increased in normal baroreflex and in the artificial baroreflex system.

V. Conclusion

The artificial baroreflex system fully restored volume buffering function as well as arterial pressure regulation. The artificial baroreflex system would be an attractive therapeutic tool in preventing pulmonary edema in the presence of baroreflex failure irrespective of left ventricular systolic function. In order to develop a clinically useful system, further inventions in developing durable pressure sensors and electrodes are essential [3].

Acknowledgment

This study was supported in part by Health and Labour Sciences Research Grant for Research on Medical Devices for Improving Impaired QOL from the Ministry of Health Labour and Welfare of Japan, Health and Labour Sciences Research Grant for Clinical Research from the Ministry of Health Labour and Welfare of Japan, and Grant-in-Aid for Scientific Research(S) (18100006) from the Japan Society for the Promotion of Science.

References

[1] Owan TE, Hodge DO, Herges RM, Jacobsen SJ, Roger VL, Redfield MM. Trends in prevalence and outcome of heart failure with preserved ejection fraction. The New England journal of medicine. 2006;355(3):251-259.

[2] Sato T, Kawada T, Miyano H, Shishido T, Inagaki M, Yoshimura R, Tatewaki T, Sugimachi M, Alexander J, Jr., Sunagawa K. New simple methods for isolating baroreceptor regions of carotid sinus and aortic depressor nerves in rats. The American journal of physiology. 1999;276(1 Pt 2):H326-332.

[3] Sugimachi M, Sunagawa K. Bionic Cardiology: Exploration Into a Wealth of Controllable Body Parts in the Cardiovascular System. IEEE REVIEWS IN BIOMEDICAL ENGINEERING. 2009:2:172-186.

33rd Annual International Conference of the IEEE EMBS
Boston, Massachusetts USA, August 30 - September 3, 2011

Consideration on Step Duration to Assess Open-loop Static Characteristics of the Carotid Sinus Baroreflex in Rats

Toru Kawada, Shuji Shimizu, Yusuke Sata, Atsunori Kamiya, Kenji Sunagawa, and Masaru Sugimachi

Abstract—**The carotid sinus baroreflex is one of the most important negative feedback systems to stabilize arterial pressure. Although static characteristics of the carotid sinus baroreflex can be assessed by using a stepwise input protocol under baroreflex open-loop conditions, the step duration has been determined empirically. In the present study, we examined the effects of different time windows (5-10, 15-20, 25-30, 35-40, 45-50, and 55-60 s) on the static characteristics estimated by using a 60-s stepwise input protocol in 10 anesthetized rats. Based on the results, we compared the static characteristics between actual 60-s and 20-s stepwise input protocols. Most of the parameters of the static characteristics did not differ significantly between the 60-s and 20-s stepwise input protocols, suggesting that the open-loop baroreflex static characteristics can be estimated by using a stepwise input with the step duration as short as 20 s in normal rats.**

I. Introduction

The carotid sinus baroreflex system is one of the most important negative feedback systems to stabilize arterial pressure (AP). The carotid sinus baroreflex may be divided into two principal subsystems [1], [2]. One is a neural arc subsystem that acts as a controller for regulating sympathetic nerve activity (SNA) in response to a baroreceptor pressure input. The other is a peripheral arc subsystem that serves as a plant for yielding AP according to SNA through cardiovascular responses. In order to assess the open-loop static characteristics of these two subsystems, a stepwise (staircase-wise) input has been employed. The levels of input pressure are changed stepwise to cover the whole input pressure range of the arterial baroreflex, e.g., between 60 and 180 mmHg in rats. Each input pressure level is sustained for certain duration to make the system response reach steady state at a given input pressure level. Empirically, 60-s step duration seems to be appropriate for estimating the baroreflex static characteristics in rats [3], [4]. Although minimizing the step duration would contribute to shortening the total experimental time, too short duration can violate the assumption of acquiring the steady-state response. In the present study, we examined possible shortest step duration necessary for estimating the baroreflex open-loop static characteristics in rats.

Manuscript received March 20, 2011. This work was supported in part by Health and Labour Sciences Research Grants (H19-nano-Ippan-009, H20-katsudo-Shitei-007, H21-nano-Ippan-005) from the Ministry of Health, Labour and Welfare of Japan.

T. Kawada, S. Shimizu, Y. Sata, and M. Sugimachi are with the Department of Cardiovascular Dynamics, National Cerebral and Cardiovascular Center, 565-8565 Osaka, Japan (corresponding author: T. Kawada, phone: +81-6-6833-5012, fax: +81-6-6835-5403, e-mail: torukawa@res.ncvc.go.jp).

K. Sunagawa is with the Department of Cardiovascular Medicine, Graduate School of Medical Sciences, Kyushu University, Fukuoka 812-8582, Japan.

II. Materials and Methods

A. Animal Preparation

Animals were cared for in strict accordance with the *Guiding Principles for the Care and Use of Animals in the Field of Physiological Sciences*, which has been approved by the Physiological Society of Japan. All experimental protocols were reviewed and approved by the Animal Subjects Committee at National Cerebral and Cardiovascular Center.

The study was conducted using ten male Sprague-Dawley rats. Each rat was anesthetized by an intraperitoneal injection (2 ml/kg) of a mixture of urethane (250 mg/ml) and α-chloralose (40 mg/ml), and mechanically ventilated through a tracheal tube with oxygen-enriched room air. A venous catheter was inserted into the right femoral vein for a maintenance dose of the above anesthetic mixture diluted by 20 fold (2-3 $ml \cdot kg^{-1} \cdot h^{-1}$). An arterial catheter was inserted into the right femoral artery to measure AP, from which heart rate (HR) was detected. Another venous catheter was inserted into the left femoral vein for the infusion of Ringer solution (6 $ml \cdot kg^{-1} \cdot min^{-1}$) to maintain fluid balance.

In order to record SNA, a postganglionic branch from the splanchnic sympathetic nerve was exposed through a left flank incision. A pair of stainless steel wire electrodes (Bioflex wire, AS633, Cooner Wire, CA, USA) was attached to the nerve, and the nerve and electrodes were covered with silicone glue (Kwik-Sil, World Precision Instruments, FL, USA). To quantify the nerve activity, the preamplified signal was band-pass filtered at 150-1000 Hz, and was full-wave rectified and low-pass filtered with a cut-off frequency of 30 Hz. Pancuronium bromide (0.4 $mg \cdot kg^{-1} \cdot h^{-1}$) was administered to prevent muscular activity from contaminating the SNA recording. At the end of the experiment, an intravenous bolus injection of a ganglionic blocker, hexamethonium bromide (60 mg/kg), was given to confirm the disappearance of SNA. The noise level was then recorded and served as zero SNA. Because the absolute magnitude of SNA varied among animals depending on recording conditions, mean SNA value corresponding to the carotid sinus pressure (CSP) of 60 mmHg calculated at the time window of 55-60 s was assigned to be 100 au (arbitrary units).

Bilateral vagal and aortic depressor nerves were sectioned at the neck to avoid reflexes from the cardiopulmonary region

and aortic arch. The carotid sinus regions were isolated from the systemic circulation using previously reported procedures [5], [6] with modifications. A 7-0 polypropylene suture with a fine needle (PROLENE, Ethicon, GA, USA) was passed through the tissue between the external and internal carotid arteries, and the external carotid artery was ligated close to the carotid bifurcation. The internal carotid artery was embolized by the injection of two to three steel balls with a diameter of 0.8 mm (Tsubaki Nakashima, Nara, Japan) via the common carotid artery. The isolated carotid sinuses were filled with warmed Ringer solution via the catheter inserted into the common carotid arteries. CSP was controlled using a servo-controlled piston pump. Heparin sodium (100 U/kg) was given intravenously to prevent blood coagulation. Body temperature was maintained at approximately 38°C with a heating pad and a lamp.

B. Estimation of Baroreflex Open-loop Static Characteristics Using Different Time Windows in a 60-s Stepwise Input

To estimate the open-loop static characteristics of the total baroreflex, neural arc, peripheral arc, and HR control, CSP was first decreased to 60 mmHg for four min, and increased stepwise from 60 to 180 mmHg at increments of 20 mmHg every minute.

Mean values of SNA, AP, and HR were calculated from time windows of 5-10, 15-20, 25-30, 35-40, 45-50, and 55-60 s at each CSP level. In each rat, data from two consecutive 60-s stepwise input cycles were averaged. The static characteristics of the total baroreflex (the CSP-AP relationship), neural arc (the CSP-SNA relationship), and HR control (the CSP-HR relationship) were quantified using a four-parameter logistic function as [7]:

$$y = \frac{P_1}{1+\exp[P_2(x-P_3)]} + P_4$$

where x and y denote the input and output values, respectively; P_1 is the response range; P_2 is the slope coefficient, P_3 is the midpoint input pressure; and P_4 is the minimum value of the output.

The static characteristics of the baroreflex peripheral arc (the SNA-AP relationship) were quantified by a linear regression analysis as:

$$AP = a \times SNA + b$$

where a and b represent the slope and intercept, respectively.

C. Estimation of Baroreflex Open-loop Static Characteristics Using a 20-s Stepwise Input

Based on preliminary results of the open-loop static characteristics using different time windows in a 60-s stepwise input described above, the system response to a 20-s stepwise input was examined. The 20-s stepwise input protocol was conducted before (n = 5) or after (n = 5) the 60-s stepwise input protocol to make the possible time effect be even between the two protocols. Mean values of SNA, AP, and HR were obtained during the last 5 s (15-20 s) at each CSP level. In each rat, data from two consecutive 20-s stepwise input cycles were averaged.

D. Statistical Analysis

All data are expressed as means±SE values. To compare the effects of differing the time windows of analysis (5-10, 15-20, 25-30, 35-40, 45-50, and 55-60 s) on the parameters of the baroreflex static characteristics, repeated-measures analysis of variance (ANOVA) was used [8]. If there was a significant difference, a Dunnett's test was applied to identify the difference against the data calculated from a time window of 55-60 s. To compare the parameters of the baroreflex static characteristics between the 60-s and 20-s stepwise input protocols, a paired-t test was used. Differences were considered to be significant when $P < 0.05$. We used a rule of thumb that the parameters derived from two protocols were considered to be similar when $P > 0.2$.

III. Results and Discussion

Fig. 1 represents typical recordings of CSP, SNA, AP, and HR during 60-s and 20-s stepwise input protocols. A white line in the SNA recording is a 2-s moving averaged signal. An increase in CSP decreased SNA, AP, and HR. The maximum and minimum values of SNA, AP, and HR responses did not differ significantly between the two input protocols.

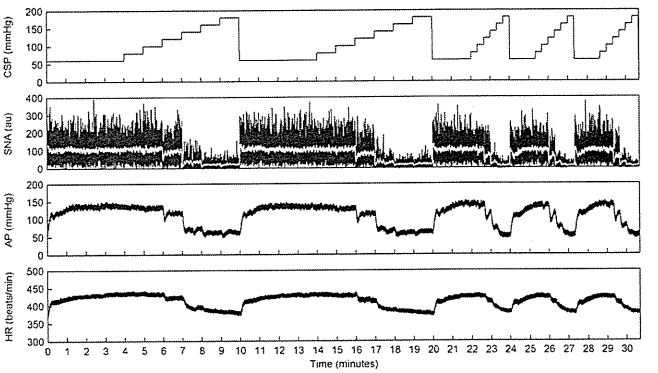

Fig. 1. Typical experimental recordings during 60-s and 20-s stepwise input protocols. CSP: carotid sinus pressure, SNA: sympathetic nerve activity, AP: arterial pressure, HR: heart rate. The white line in the SNA recording represents a 2-s moving averaged signal.

Figure 2 (the last page) summarizes the open-loop static characteristics of the total baroreflex, neural arc, peripheral arc, and HR control, obtained from the 60-s stepwise input protocol, with the analyses using different time windows. The characteristics of the total baroreflex, neural arc, and HR control approximated an inverse sigmoid curve. The characteristics of the peripheral arc approximated a straight line. The data obtained during 55-60 s served as controls. The estimated parameter values, except those estimated during 5-10 s, did not differ significantly from those obtained during 55-60 s (Table 1), suggesting that the open-loop static characteristics of the baroreflex could be obtained using a stepwise input with step duration as short as 20 s.

Figure 3 (the last page) compares the open-loop static characteristics of the total baroreflex, neural arc, peripheral arc, and HR control between actually applied 20-s and 60-s stepwise input protocols. Data were calculated from the last 5 s of each step. The lines of mean data obtained from the two protocols were very close (Fig. 3, right panels, dashed line: 20-s, solid line: 60-s). In the parameters of the total baroreflex, no significant differences were detected between the two protocols (Table 2). In the neural arc, although the slope coefficient was significantly smaller by 0.006 in the 20-s stepwise input protocol, the magnitude of the difference was comparable to the corresponding SE value (0.006) in the 60-s stepwise input protocol. Other parameters of the neural arc did not differ significantly. Parameters of the peripheral arc did not differ significantly between the two protocols. In the HR control, although the response range was significantly smaller by 3.6 beats/min in the 20-s stepwise input protocol, the magnitude of the difference was less than the corresponding SE value (7.5 beats/min) in the 60-s stepwise input protocol. Other parameters did not differ significantly. Although we did not carry out an equivalence test, if we use a rule of thumb that the two parameter values are considered to be similar when $P > 0.2$, the midpoint input pressure (P_3) could be different in all of the total baroreflex, neural arc, and the HR control. The percent difference of P_3 values relative to the value estimated by the 60-s stepwise input protocol was, however, less than 5% on the average. Collectively, although several parameters differed slightly, the 20-s stepwise input protocol provided parameter values similar to those obtained from the 60-s stepwise input protocol. The differences of the parameters between the two protocols could not be detected if we applied an unpaired-t test instead of a paired-t test, suggesting that the detected difference was within the inter-individual variations.

Although too short step duration in a stepwise input protocol will violate the assumption that the system's steady-state response is obtained, too long step duration will also violate the assumption that the system remains stationary. Minimizing the step duration may contribute to shortening the total experimental time and making the assumption for stationarity more feasible in biological experiment. In addition, when examining the effects of certain interventions on the system characteristics, reducing the step duration would increase the time resolution for tracking the effects of interventions on the system characteristics. In other words, by using a 20-s stepwise input protocol, we may be able to increase the time resolution of the systems analysis by 3 fold compared to a 60-s stepwise input protocol.

There is a limitation to the present study. We estimated the baroreflex static characteristics in normal anesthetized rats. In diseased conditions such as chronic heart failure, the cardiovascular responses could be blunted [3]. In such conditions, longer step duration may be required for AP to reach a new steady state at a given input pressure, and thus the 20-s stepwise input protocol may not work well. Apparently, some priori knowledge or preliminary studies are needed to use the 20-s rather than the 60-s stepwise input protocol.

IV. Conclusion

The open-loop static characteristics of the carotid sinus baroreflex in normal rats may be obtained by the stepwise input protocol with step duration as short as 20 s. The shortening of the step duration can reduce the total amount of experimental time. Moreover, it would also make it possible to analyze the time effect of drugs on the baroreflex static characteristics with a better time resolution.

References

[1] D. E. Mohrman, L. J. Heller. Cardiovascular Physiology, 6th ed. New York: Lange Medical Books/McGraw-Hill, 2006, pp. 172–177.

[2] T. Sato, T. Kawada, M. Inagaki, T. Shishido, H. Takaki, M. Sugimachi, et al. "New analytic framework for understanding sympathetic baroreflex control of arterial pressure," *Am. J. Physiol.*, vol. 276, pp. H2251-H2261, 1999.

[3] T. Kawada, M. Li, A. Kamiya, S. Shimizu, K. Uemura, H. Yamamoto, et al. "Open-loop dynamic and static characteristics of the carotid sinus baroreflex in rats with chronic heart failure after myocardial infarction," *J. Physiol. Sci.*, vol. 60, pp. 283-298, 2010.

[4] T. Kawada, A. Kamiya, M. Li, S. Shimizu, K. Uemura, H. Yamamoto, et al. "High levels of circulating angiotensin II shift the open-loop baroreflex control of splanchnic sympathetic nerve activity, heart rate and arterial pressure in anesthetized rats," *J. Physiol. Sci.*, vol. 59, pp. 447-455, 2010.

[5] A. A. Shoukas, C. A. Callahan, J. M. Lash, E. B. Haase. "New technique to completely isolate carotid sinus baroreceptor regions in rats," *Am. J. Physiol. Heart Circ. Physiol.*, vol. 260, pp. H300-H303, 1991.

[6] T. Sato, T. Kawada, H. Miyano, T. Shishido, M. Inagaki, R. Yoshimura, et al. "New simple methods for isolating baroreceptor regions of carotid sinus and aortic depressor nerves in rats," *Am. J. Physiol. Heart Circ. Physiol.*, vol. 276, pp. H326-H332, 1999.

[7] B. B. Kent, J. W. Drane, B. Blumenstein, J. W. Manning. "A mathematical model to assess changes in the baroreceptor reflex," *Cardiology.*, vol. 57, pp. 295-310, 1972.

[8] S. A. Glantz, Primer of Biostatistics, 5th ed. New York: McGraw-Hill, 2002, pp. 318-329.

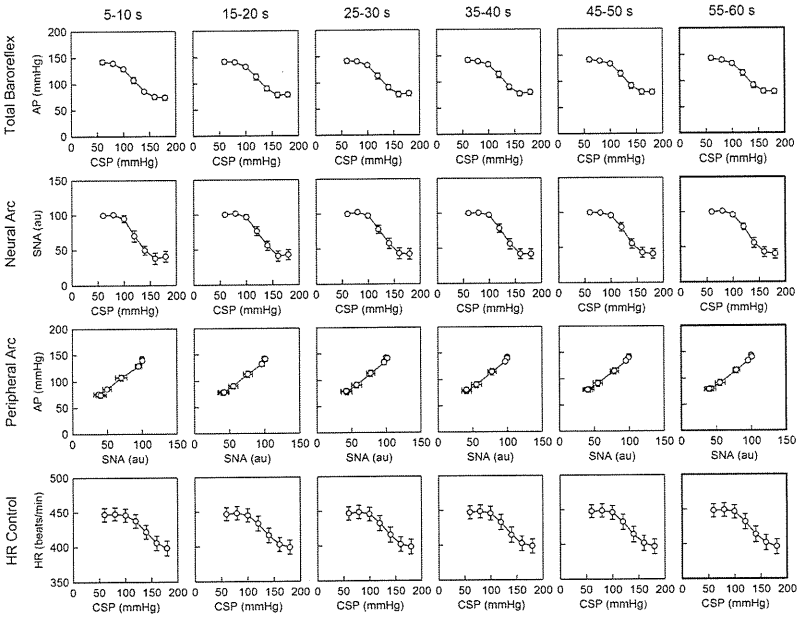

Fig. 2. Open-loop static characteristics of the carotid sinus baroreflex estimated at different time windows of the 60-s stepwise input protocol. CSP: carotid sinus pressure, AP: arterial pressure, SNA: sympathetic nerve activity, HR: heart rate. The rightmost panels serve as controls.

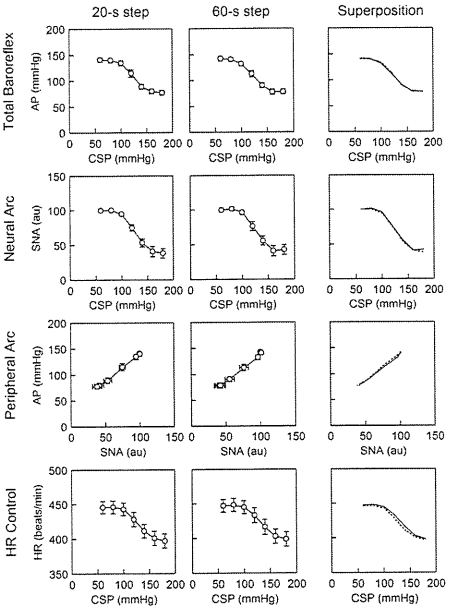

Fig. 3. Open-loop static characteristics of the carotid sinus baroreflex estimated using 20-s and 60-s stepwise input protocols. CSP: carotid sinus pressure, AP: arterial pressure, SNA: sympathetic nerve activity, HR: heart rate.

Table 1. Parameters of open-loop static characteristics of the carotid sinus baroreflex estimated at different time windows in the 60-s stepwise input protocol.

	5-10 s	15-20 s	25-30 s	35-40 s	45-50 s	55-60 s
Total Baroreflex						
P_1, mmHg	72.5±8.6**	68.8±8.0	67.9±7.8	66.4±7.7	65.0±7.8	65.4±7.1
P_2, mmHg^{-1}	0.088±0.011	0.089±0.009	0.095±0.011	0.099±0.009	0.097±0.009	0.091±0.008
P_3, mmHg	118.1±3.6**	122.1±3.5	122.8±3.6	123.6±3.5	124.0±3.6	123.7±3.6
P_4, mmHg	72.9±4.8**	74.9±5.2	75.1±5.2	75.5±5.1	76.2±5.1	76.3±4.8
Neural Arc						
P_1, au	65.5±7.6	63.0±6.7	62.6±8.0	62.8±7.3	61.3±7.1	63.1±6.5
P_2, mmHg^{-1}	0.115±0.014	0.102±0.012	0.102±0.010	0.100±0.009	0.101±0.010	0.088±0.006
P_3, mmHg	120.6±3.6**	125.1±3.7	126.0±3.8	127.8±3.8	127.2±3.6	127.0±3.6
P_4, au	37.6±7.8	39.3±7.4	40.1±8.1	38.4±7.3	39.3±7.1	38.7±6.7
Peripheral Arc						
a, mmHg/au	1.06±0.07	1.06±0.07	1.10±0.07	1.09±0.08	1.07±0.07	1.06±0.07
b, mmHg	31.0±7.4	31.2±6.9	27.0±8.0	29.4±8.1	32.0±6.4	32.1±7.0
HR Control						
P_1, beats/min	52.8±8.2	51.8±8.4	52.3±8.2	51.7±8.0	53.8±8.0	54.8±7.5
P_2, mmHg^{-1}	0.077±0.006	0.082±0.008	0.089±0.010	0.093±0.009	0.087±0.008	0.083±0.007
P_3, mmHg	138.5±2.9**	131.0±3.1	131.0±3.4	130.5±3.3	131.1±3.6	130.8±3.5
P_4, beats/min	395.7±10.8	397.2±10.4	396.8±10.8	397.4±10.3	395.7±10.6	395.2±10.5

Data are means±SE values. **P < 0.01 by Dunnett's test from the value estimated at a time window of 55-60 s.

Table 2. Parameters of open-loop static characteristics of the carotid sinus baroreflex estimated by actual 20-s and 60-s stepwise input protocols.

	20-s step	60-s step	P value	%difference
Total Baroreflex				
P_1, mmHg	65.9±7.5	65.4±7.1	0.779	0.1±3.5
P_2, mmHg^{-1}	0.094±0.009	0.091±0.008	0.691	1.0±8.1
P_3, mmHg	121.9±3.0	123.7±3.6	0.148	1.4±0.9
P_4, mmHg	76.6±4.3	76.3±4.8	0.893	−0.4±2.0
Neural Arc				
P_1, au	65.5±7.6	63.1±6.5	0.330	−1.5±4.5
P_2, mmHg^{-1}	0.082±0.008*	0.088±0.006	0.011	10.8±3.8
P_3, mmHg	121.8±3.3	127.0±3.6	0.075	4.4±2.3
P_4, au	37.4±7.2	38.7±6.7	0.414	9.6±7.5
Peripheral Arc				
a, mmHg/au	1.09±0.08	1.06±0.07	0.351	−1.1±2.5
b, mmHg	31.4±8.3	32.1±7.0	0.780	7.3±11.1
HR Control				
P_1, beats/min	51.2±8.2*	54.8±7.5	0.041	13.7±7.6
P_2, mmHg^{-1}	0.082±0.008	0.083±0.007	0.820	6.6±8.9
P_3, mmHg	126.5±3.3	130.8±3.5	0.126	3.5±2.1
P_4, beats/min	396.4±10.4	395.2±10.5	0.501	−0.3±0.4

Data are means±SE values. *P < 0.05 by a paired-t test.